Topologically protected braiding in a single wire using Floquet Majorana modes –Supplementary Material—

Bela Bauer,[1] T. Pereg-Barnea,[2,3] Torsten Karzig,[1] Maria-Theresa Rieder,[3] Gil Refael,[4,5] Erez Berg,[3,6] and Yuval Oreg[3]

[1] *Station Q, Microsoft Corporation, Santa Barbara, California 93106 USA*
[2] *Department of Physics, McGill University, Montréal, Québec, Canada*
[3] *Department of Condensed Matter Physics, Weizmann Institute of Science, Rehovot 76100, Israel*
[4] *Walter Burke Institute for Theoretical Physics and Institute for Quantum Information and Matter, California Institute of Technology, Pasadena, California 91125 USA*
[5] *Department of Physics, California Institute of Technology, Pasadena, California 91125 USA*
[6] *Department of Physics, James Franck Institute, University of Chicago, Chicago, Illinois 60637 USA*

(Dated: April 4, 2019)

SUPPLEMENTAL MATERIAL

A. The sweet spots

In this section we revisit the 'sweet spots' mentioned in the main text. The 'sweet spots' describe locations in the phase diagram where both MZM and MPM are localized on one or two sites, i.e. the correlation length vanishes. Let us provide a simple analytical approach to deriving these sweet spots. First, let us denote each Dirac Fermion operator c by two Majorana operators a and b on each site. Formally we substitute $2c_n = a_n + ib_n$ with $\{a_n, b_m\} = 0$ for all n and m and $a_n^2 = b_n^2 = 1$. (These are related to $\vec{\gamma}$ introduced in the main text by $a_n = \gamma_{2n-1}$, $b_n = \gamma_{2n}$.) Then the model becomes

$$H_0 = -i\frac{\pi}{T}\lambda_0 \sum_{n=1}^{N-1} a_{n+1}b_n \quad H_1 = -i\frac{\pi}{T}\lambda_1 \sum_{n=1}^{N} a_n b_n, . \quad (1)$$

This model is depicted in Fig. 1.

We note that application of $e^{-iH_0T/2}$ with $\lambda_0 = 1/2$ exchanges the positions of b_n and a_{n+1} for $n = 1, 2, \ldots, N-1$. Indeed, defining

$$U_0 \equiv e^{\frac{\pi}{4}\sum_{n=1}^{N-1} b_n a_{n+1}} = \Pi_{n=1}^{N-1} B_0^n, \; B_0^n = e^{\frac{\pi}{4} b_n a_{n+1}}, \quad (2)$$

one can readily check that

$$B_0^{n\dagger} b_n B_0^n = a_{n+1} \text{ and } B_0^{n\dagger} a_{n+1} B_0^n = -b_n. \quad (3)$$

Notice that B_0^n and B_0^m commute for $n \neq m$. Similarly

$$U_1 \equiv e^{\frac{\pi}{4}\sum_{n=1}^{N} a_n b_n} = \Pi_{n=1}^{N} B_1^n, \text{ and } B_1^n = e^{\frac{\pi}{4} a_n b_n}, \quad (4)$$

and

$$B_1^{n\dagger} b_n B_1^n = a_n, \text{ and } B_1^{n\dagger} a_n B_1^n = -b_n. \quad (5)$$

These operations are depicted in Fig. 1. The arrow indicates which Majorana operator acquires the minus sign. For example, in the application of U_1 (green arrows in Fig. 1), $b_n \to a_n$ as the arrow directed from b_n to a_n while $a_n \to -b_n$.

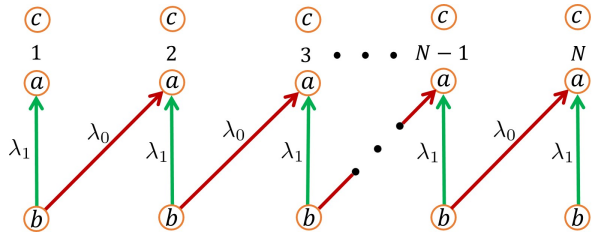

FIG. 1. The Hamiltonian Eq. (1). Red links represent H_0, and green links H_1. An application of $U_0 \equiv e^{-iH_0T/2}$ with $\lambda_0 = 1/2$ exchanges the positions of the MZM b_n and a_{n+1} yielding $b_n \to a_{n+1}$ and $a_{n+1} \to -b_n$. Similarly, $U_1 \equiv e^{-iH_1T/2}$ with $\lambda_1 = 1/2$ carries out the transformation $a_n \to b_n$ and $b_n \to -a_n$. The four sweet spots (indicated by crosses in the left panel of Fig. 1 of the main text) are obtained by successive application of U_0, U_1 and the identity operator (i.e., a vanishing Hamiltonian for time $T/2$) $I = e^{-iH_0T/2} = e^{-iH_1T/2}$ with $\lambda_0 = \lambda_1 = 0$. The trivial phase is obtained with the application of IU_1. The MZM phase, which contain MZM only, is obtained with the application of U_0I. The MPM phase, which has only π modes, is obtained with the application of $U_0U_1^2$. Finally, the MZM and MPM phase, having both zero and π Majorana modes is obtained with the application of $U_0^2U_1$. Notice that the application of $U_{0(1)}$ twice is equivalent to taking $e^{-iH_{0(1)}T/2}$ but now with $\lambda_{0(1)} = 1$.

Using these observations, and the identity operator (a vanishing Hamiltonian for $T/2$) $I = e^{-iH_0T/2} = e^{-iH_1T/2}$ with $\lambda_0 = \lambda_1 = 0$, it is now straightforward to identified the operation of the Floquet operator $U_F = e^{-iH_0T/2}e^{-iH_1T/2}$ at the sweet spots in the various phases.

1. 1. *Trivial*

The trivial phase is obtained with the application of IU_1 (corresponding to $\lambda_0 = 0, \lambda_1 = 1/2$) then:

$$a_n \xrightarrow{I} a_n \xrightarrow{U_1} -b_n \text{ and } b_n \xrightarrow{I} b_n \xrightarrow{U_1} a_n$$

for $n = 1, \ldots, N$. So that in the subspace spanned by a_n and b_n the operator $\vec{v}_n \cdot (a_n, b_n)^T$ evolves into $(\bar{U}_F \vec{v}_n) \cdot (a_n, b_n)^T$, with

$$\bar{U}_F = \begin{pmatrix} 0 & 1 \\ -1 & 0 \end{pmatrix} = i\sigma_y,$$

having eigenvalues $\pm i = e^{\pm i\epsilon_n T}$ with quasi-energies $\epsilon_n = \pm\pi/(2T)$ for all n, which are not corresponding to Majorana modes, occurring at quasi-energies zero or π/T.

2. 2. MZM

The phase with MZM only at the two ends of the wire is obtained with the application of $U_0 I$ (corresponding to $\lambda_0 = 1/2, \lambda_1 = 0$) then:

$$a_{n+1} \xrightarrow{U_0} -b_n \xrightarrow{I} -b_n \text{ and } b_n \xrightarrow{U_0} a_{n+1} \xrightarrow{I} a_{n+1},$$

for $n = 1, \ldots N-1$. So that in the subspace spanned by a_{n+1} and b_n (for $n = 1, \ldots, N-1$) we find, similarly to the trivial case, quasi-energies $\pm\pi/(2T)$, but the Majorana operators a_1 and b_N remain unchanged, establishing the presence of two MZM modes which are localized on one site. In the subspace spanned by a_1 and b_N we find that $\bar{U}_F$ is the identity matrix with eigenvalues $1 = e^{i\epsilon T}$, and two quasi-energies $\epsilon = 0$.

3. 3. MPM

The phase with MPM only at the two ends of the wire is obtained with the application of $U_0 U_1^2$ corresponding to $\lambda_0 = 1/2, \lambda_1 = 1$; notice that the application of $U_{0(1)}$ twice is equivalent to taking $e^{-iH_{0(1)}T/2}$ with $\lambda_{0(1)} = 1$, and results in the multiplication of the Majorana operator by -1. Then,

$$\begin{aligned} a_{n+1} &\xrightarrow{U_0} -b_n \xrightarrow{(U_1)^2} b_n, \text{ and} \\ b_n &\xrightarrow{U_0} a_{n+1} \xrightarrow{(U_1)^2} -a_{n+1}, \end{aligned}$$

for $n = 1, \ldots N-1$. So that in the subspace of a_{n+1} and b_n (for $n = 1, \ldots, N-1$) we find $\bar{U}_F = -i\sigma_y$, and similarly to the trivial case the corresponding quasi-energies $\pm\pi/(2T)$. The Majorana operators a_1 and b_N are special:

$$\begin{aligned} a_1 &\xrightarrow{U_0} a_1 \xrightarrow{(U_1)^2} -a_1 \text{ and} \\ b_N &\xrightarrow{U_0} b_N \xrightarrow{(U_1)^2} -b_N. \end{aligned}$$

In the subspace of a_1 and b_N we find that $\bar{U}_F$ is equal to the negative of the identity matrix whose two eigenvalues are $-1 = e^{i\epsilon T}$, and two quasi-energies $\epsilon = \pi/T$. This corresponds to MPMs localized at the first and last site of the system.

4. 4. MZM and MPM

The phase with MZM and MPM at the two ends of the wire is obtained with the application of $U_0^2 U_1$ (corresponding to $\lambda_0 = 1, \lambda_1 = 1/2.$) then:

$$\begin{aligned} a_n &\xrightarrow{(U_0)^2} -a_n \xrightarrow{U_1} b_n \text{ and} \\ b_n &\xrightarrow{(U_0)^2} -b_n \xrightarrow{U_1} -a_n, \end{aligned}$$

for $n = 2, \ldots N-2$. In the subspace of a_n and b_n we find $\bar{U}_F = i\sigma_y$ with quasi-energies $\pm\pi/(2T)$. The Majorana operators a_1, b_1 and a_N, b_N are special:

$$\begin{aligned} a_1 &\xrightarrow{(U_0)^2} a_1 \xrightarrow{U_1} -b_1, \\ b_1 &\xrightarrow{(U_0)^2} -b_1 \xrightarrow{U_1} -a_1, \\ a_N &\xrightarrow{(U_0)^2} -a_N \xrightarrow{U_1} b_N, \text{ and} \\ b_N &\xrightarrow{(U_0)^2} b_N \xrightarrow{U_1} a_N. \end{aligned}$$

In the subspace of a_1 and b_1 we find that $\bar{U}_F = -\sigma_x$ with eigenvalues $\mp 1 = e^{i\epsilon T}$, and two quasi-energies $\epsilon = \pi/T$ and $\epsilon = 0$. The corresponding eigen-oprators are $(a_1 + b_1)/\sqrt{2}$ and $(a_1 - b_1)/\sqrt{2}$, respectively. Similarly, in the subspace of a_N and b_N we find that $\bar{U}_F = \sigma_x$ with eigenvalues $\pm 1 = e^{i\epsilon T}$, and two quasi-energies $\epsilon = 0$ and $\epsilon = \pi/T$, and the corresponding eigen-oprators are $(a_1 + b_1)/\sqrt{2}$ and $(a_1 - b_1)/\sqrt{2}$, respectively. We therefore find Majorana zero and π modes as symmetric and anti-symmetric superpositions of the elementary Majorana operators at the first and last sites of the system.

B. Local time-translation symmetry breaking

As discussed in the main manuscript, we couple nearby MZMs and MPMs by introducing a local operator U_{pert} after every two elementary Floquet cycles. In the case where there is no adiabatic change of the drive parameters, this amounts simply to changing U_F^n to $\left(U_F^2 U_{\text{pert}}\right)^{n/2}$.

To confirm this picture, we turn to numerical simulations, which we perform using established techniques [1]. We compute the spectrum of the operator $U_F(\delta)^2 U_{\text{pert}}$, where $U_F(\delta)$ is the Floquet operator of Eq. 2 of the main text with the parameters chosen inside phase 4 which exhibits both zero and π modes, and U_{pert} acting only on one half of the system. Specifically, we choose

$$U_{\text{pert}}(\lambda_{\text{pert}}) = e^{iTH(T\mu_i = \lambda_{\text{pert}}, Tw_i = \lambda_{\text{pert}}, T\Delta_i = -\lambda_{\text{pert}})}, \quad (6)$$

where μ_i, w_i and Δ_i are non-vanishing only in the right half of the system. For $\lambda_{\text{pert}} = 0$, time-translation symmetry for a single Floquet cycle is restored and the system will exhibit two localized and uncoupled modes at each end. However, when $\lambda_{\text{pert}} > 0$, the (0 and π) modes at the right end split, while the MZM and MPM at the

left remain as the only unsplit modes. This behavior is reflected in the spectrum shown in Fig. 2, which shows the lowest (in absolute value) quasi-energies of $U_F(\delta)^2 U_{\text{pert}}$ for two choices of λ_{pert}. Due to particle-hole symmetry, the positive and negative quasi energies mirror each other. For the unperturbed case, $\lambda_{\text{pert}} = 0$, we find that four eigenvalues approach zero exponentially as the system size is increased. Upon perturbing the system, two of them saturate to a value of order λ_{pert}, while the others continues to decrease exponentially with the same exponent that governed the unperturbed case.

A subtle point arises if both a perturbation that breaks time-translation symmetry is present, and the Floquet drive is slowly changed to move phase boundaries as described above. In that case the Floquet unitary of a single cycle is $U_F(s)$ with s a slowly changing parameter such that consecutive cycles are described by $U_F(s')U_F(s)$ with $s' - s = 1/N_s$. When adding a perturbation U_{pert} to this, it is important that the parameter s is still changed in every step, i.e. the perturbed evolution over two cycles is $U_{\text{pert}}U_F(s')U_F(s)$. The perturbation will still be effective as long as $U_F(s)$ and $U_F(s')$ are sufficiently close. While it may appear more natural to change the parameter s only every two cycles when inserting the perturbation, such a protocol would inadvertently introduce an additional half-frequency perturbation which may lead to errors even in the limit of $N_s \to \infty$. Similar corrections may be explicitly exploited to perform certain geometric quantum gates [2, 3].

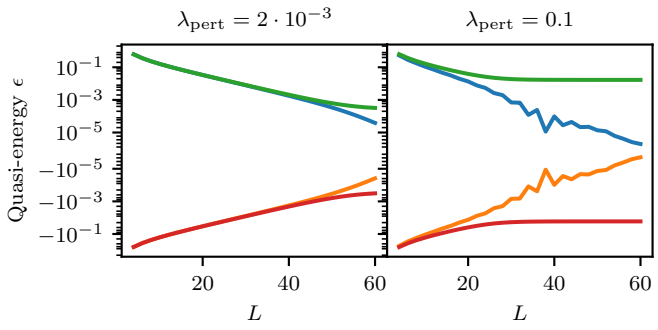

FIG. 2. Quasi energies closest to zero for Floquet evolutions over two cycles for a system of length L in phase 4 ($\delta = 0.09$) for different strengths of time-translational symmetry breaking perturbations applied the right end of the system. Left, right panel show the case of a very weak ($\lambda_{\text{pert}} = 2 \cdot 10^{-3}$) and moderate perturbation ($\lambda_{\text{pert}} = 0.1$), respectively. In the unperturbed case, each level is two-fold degenerate corresponding to two MZMs and two MPMs. In the perturbed case, since the pair of MZM and MPM at the right end of the system is split, only the MZM and MPM at the left end remains. Notice that when $\lambda_{\text{pert}} \neq 0$ the period is doubled, and as a result the MZMs and MPMs both get folded to the vicinity of $\epsilon = 0$.

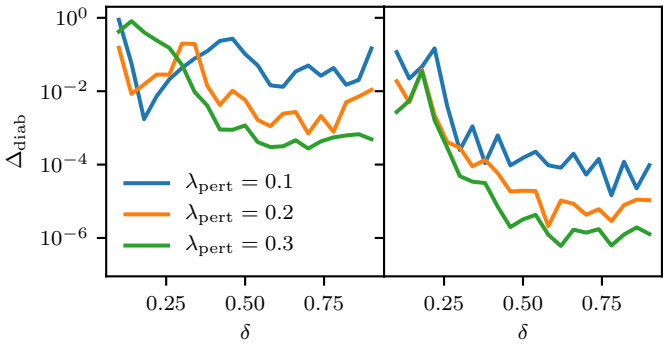

FIG. 3. Diabatic errors for two different values of N_s (left panel: $N_s = 125$, right panel: $N_s = 500$) as a function of δ, the deviation from the critical point, for different strengths of the perturbation used to split the extra pair of MZM and MPM, λ_{pert}. $\delta = 1$ corresponds to the limit of vanishing correlation length. System size is $L = 120$. It is important to note that δ controls the correlation length and the spectral gap, and therefore also bounds the gap induced by the perturbation. For the system size used here, finite-size corrections are less prevalent than diabatic errors.

C. Numerical methods

We now review the method by which we calculate the time evolution of the system. In any time step our Hamiltonian is bilinear in the Majorana operators γ_i and we write its general form as

$$H_{ij}(t) = \vec{\gamma}^T \bar{J} \vec{\gamma} \tag{7}$$

where $\vec{\gamma}$ is a column vector of Majorana operators and $\bar{J}$ is an antisymmetric imaginary matrix. (We denote matrices of c-numbers with an overbar.) The time evolution operator contains an exponent of the Hamiltonian and acts on the Majorana operators. Let us denote by $\vec{v}_j$ the eigenvectors of $\bar{J}$ with corresponding eigenvalues v_j. We can express any linear combination of Majorana operators as $V = \vec{V} \cdot \vec{\gamma} = \sum_j \alpha_j \vec{v}_j \cdot \vec{\gamma}$. The action of the evolution operator

$$U_t = \exp\left(it\vec{\gamma}^T \bar{J} \vec{\gamma}\right)$$

on V can be written as [4]:

$$U_t V U_t^{-1} = \left(\bar{U}_t \vec{V}\right) \cdot \vec{\gamma} \tag{8}$$

$$\bar{U}_t = \exp\left(4it\bar{J}\right), \tag{9}$$

Note that the factor of 4 stems from the anticommutation relations of Majorana operators $\{\gamma_i, \gamma_j\} = 2\delta_{ij}$. Given the Hamiltonian in each time step, we exponentiate the matrices $\bar{J}(t)$ for each step and multiply them in the correct order to obtain the full time evolution operator.

D. Parametric dependence of the diabatic errors

We numerically find that the parameters that control the diabatic errors – system size L, number of steps in which the modes are moved N_s, de-tuning from the critical point δ and perturbation strength λ_{pert} – can exhibit very complicated interplay. Consider, for example, the position in the phase diagram, which we control through the distance to the critical point, δ. This parameter directly or indirectly affects many physical properties of the system and can thus have a complicated effect on the results. Its primary role is to control the spectral gap of the unperturbed Floquet operator and the correlation length of the system. This correlation length controls the exponent with which the hybridization between pairs of MZMs and pairs of MPMs falls off as the distance between them is increased (see also Fig. 2), and thus exponentially affects the splitting. At the same time, since it sets the gap of the undriven Floquet operator, which also bounds the local splitting between MZMs and MPMs that the perturbation can incur, it controls diabatic corrections.

We highlight some of this complicated interplay in Fig. 3. We observe that for small N_s (left panel), the error is largely independent of δ, i.e. how close the system is to the fixed point of vanishing correlation length (which corresponds to $\delta = 1$). For larger N_s, the error decreases as δ is increased, i.e. the system is tuned closer to the "sweet spot". However, in this regime we find that the dependence on system size is very weak (not shown). We conclude from this that the finite-size errors, in particular coming from hybridization between the MZMs and MPMs, are small compared to diabatic errors. The diabatic errors are controlled by the interplay of N_s and the minimal relevant gap, which depending on the parameters can be either the bulk gap (controlled by δ) or the gap induced between MZMs and MPMs in the perturbed region, which depends on both δ and λ_{pert}.

E. Electrostatic driving

The model described in the main manuscript assumes that all parameters of the Hamiltonian can be controlled in a time-dependent fashion. However, in more realistic situations, one would like to have to control fewer parameters. A particularly attractive scenario is to leave the pairing and the hopping time independent and vary only the on-site potential μ on each site, which in many potential realizations of p-wave superconductors is easily done. For example, in solid-state realizations, one can imagine driving the gates controlling the electrostatic environment. A more direct realization of the Kitaev chain can be implemented by a chain of superconducting quantum dots [5–7], where the potential can be tuned locally for each dot. As we show below, from a theoretical point of view tuning only the chemical potential is equally viable as the model described in the main manuscript, except that such a model does not exhibit the "sweet spot" parameters with zero correlation length for the MZMs and MPMs. We will discuss how adding the control of an additional parameters allows tuning into the sweet spot regime in section Suppl. F.

In this section we study a Floquet model in which the Kitaev Hamiltonian is applied over a period T where the chemical potential μ is varied from a value of μ_1 in one part of the cycle to a value μ_2 in the remaining part. The Floquet operator reads:

$$U = e^{-iH_1T_1}e^{-iH_2T_2} \tag{10}$$

$$H_j = \sum_i \Big[-\mu_j c_i^\dagger c_i - \frac{w}{2}\left(c_i^\dagger c_{i+1} + \text{h.c.}\right) + \frac{\Delta}{2}\left(c_i c_{i+1} + \text{h.c.}\right)\Big], \tag{11}$$

where the total Floquet period is $T = T_1 + T_2$. One can find the topological invariants of the above system by considering a ring with periodic boundary conditions and noting that at the time-reversal invariant momentum points $k = 0, \pi$ the two parts of the Floquet operator commute since the order parameter vanishes. At these points the quasi-energy is simply the time averaged kinetic energy shifted into the first Floquet zone. This allows us to simplify the general formula of Ref. 8 and write:

$$\begin{aligned} Q_0 &= (-1)^{\lfloor \overline{E_k(k=0)}T\rfloor + \lfloor \overline{E_k(k=\pi)}T\rfloor} \\ &= (-1)^{\lfloor(-\mu_1+w)\lambda T + (-\mu_2+w)(1-\lambda)T\rfloor} \\ &\times (-1)^{\lfloor(-\mu_1-w)\lambda T + (-\mu_2-w)(1-\lambda)T\rfloor} \end{aligned} \tag{12}$$

$$\begin{aligned} Q_0\cdot Q_\pi &= (-1)^{\lfloor \overline{E_k(k=0)}2T\rfloor + \lfloor \overline{E_k(k=\pi)}2T\rfloor} \\ &= (-1)^{\lfloor(-\mu_1+w)\lambda 2T + (-\mu_2+w)(1-\lambda)2T\rfloor} \\ &\times (-1)^{\lfloor(-\mu_1-w)\lambda 2T + (-\mu_2-w)(1-\lambda)2T\rfloor}. \end{aligned} \tag{13}$$

Here, $\overline{E_k(k)} = \frac{1}{T}\int_0^T(\epsilon_k(t) - \mu(t))dt$ is the kinetic energy averaged over a period T and we defined the function $\lfloor x\rfloor = \text{floor}(x/2\pi)$ that counts the number of times the band was folded back into the Floquet zone. It can be checked that Q_0 yields $-(+)1$ when zero energy is intersected by an odd(even) number of bands of the kinetic energy $\overline{E_k(k)}$ folded back into the first Floquet zone. Therefore, $Q_0 = -1$ corresponds to the topological phase with MZMs. In Eq. (13) we consider doubling the period which folds back the MPMs to zero energy. The quantity Q_0Q_π then counts the combined parity of pairs of MZMs and MPMs. Note that the first line in each invariant is more general then our stroboscopic model and can be applied to any time dependent Kitaev Hamiltonian. In addition to the stroboscopic time dependence of Eq. (10), we also consider time dependent systems where the chemical potential is of the form $\mu(t) = \mu_0 + \mu_c\cos(\Omega t)$.

Fig. 4 shows the phase diagram of the stroboscopic model when the total period T is varied as well as the relative length of the first part of the period, $\lambda = T_1/T$.

While Eqs. (12),(13) give us the topological invariants they do not predict the size of the gap which is important for the accuracy of our procedure. We therefore look

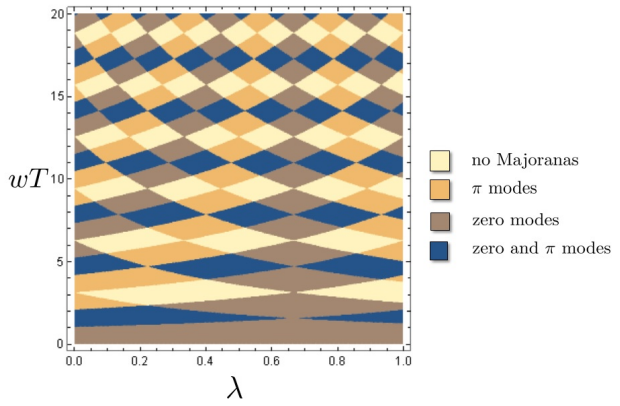

FIG. 4. The phase diagram of the stroboscopic Kitaev model when only the chemical potential μ varies between two values, $\mu_1 = -0.5w$ and $\mu_2 = w$. Both the total time T and the relative first part of the period $\lambda = T_1/T$ are varied.

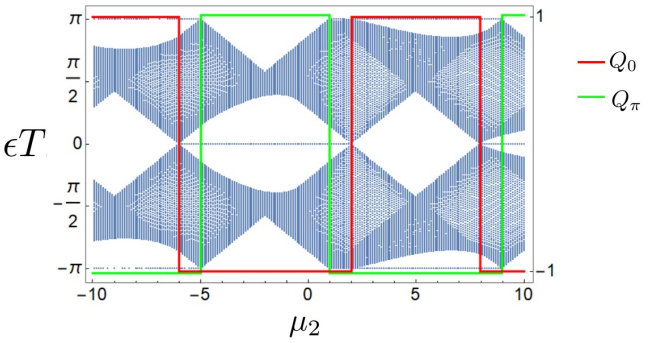

FIG. 5. The quasienergy spectrum of a finite chain in the Floquet-Majorana model (left y-axis) together with the topological invariants (right y-axis). The times T_1 and T_2 are set to 0.45, $\omega = 1$, $\mu_1 = 2$ and μ_2 is scanned.

at the stroboscopic model with an example of parameter choice where $T_1 = T_2 = T/2, \mu_1 = 2/T$ and varying μ_2. This gives us all three phases needed for our exchange procedure while the fourth one (a trivial phase) can be achieved by making $\mu_1 = \mu_2 = 2/T$ such that the system is at the trivial equilibrium phase. Fig. 5 shows all quasienergies of a finite chain (of 80 sites) as a function of the changing μ_2, together with the topological invariants Q_0 and Q_π.

Likewise we model a sinusoidal time dependent chemical potential and arrive at similar results. The quasienergy spectrum is obtained by discretizing time, i.e. calculating the time evolution over a period as the product of evolution operators over small time slices. The results are shown in Fig. 6.

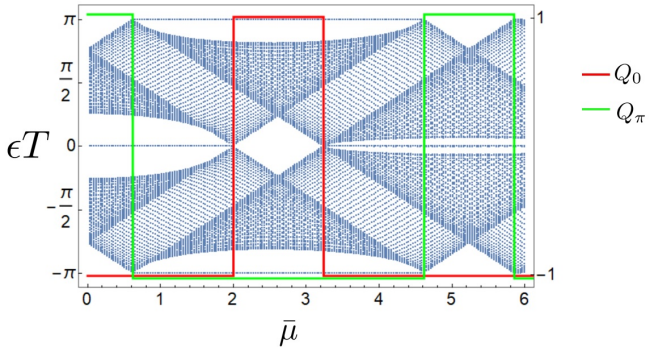

FIG. 6. The quasienergy spectrum of a finite chain in the Floquet-Majorana model (left y-axis) together with the topological invariants (right y-axis). The parameters are $T = 1.2$, $\omega = 1$ and $\mu(t) = \bar{\mu} + \mu_1 \cos(\Omega t)$ with $\mu_1 = 3$.

F. Sweet spot regime tuning with 2 parameter control

In chains of superconducting quantum dots where both the chemical potential and the tunnel coupling can be controlled the limitation to a single-parameter control is not required. This allows to tune into the sweet spot regime of each phase where the bands of the continuum states become flat. Narrow bands are useful to exploit prethermalization which avoids possible heating effects in the driven system (see, e.g., Ref. [9]). Indeed, when the available energy exchange with a single particle is limited by the band width, high-order multi-particle processes are required to relax energy between Floquet zones. For weak interactions, relaxation processes then become exponentially suppressed in the ratio of the bandwidth to the drive frequency. Figure 4 already suggests that tuning w and λ allows to access the entire phase diagram. More explicitly, Fig. 7 shows the phase diagram of a stroboscopic drive protocol (see. Eq. (10)) with fixed $T_1 = T_2$, μ_1 as a function of w and μ_2. The result is similar to the phase diagram in the main text Fig. 1 with sweet spots residing in the center of the diamonds of a particular phase. Note that similar to section Suppl. E, it is only the chemical potential term that is driven on the fast time scales of a Floquet period. The hopping parameter w would only need to be changed slowly to accomodate the braiding procedure.

[1] For an overview, see the Supplemental Material as well as Refs. [10–12].
[2] R. W. Bomantara and J. Gong, Phys. Rev. Lett. **120**, 230405 (2018).
[3] Raditya Weda Bomantara and Jiangbin Gong, Preprint (2018), arXiv:1807.07276.
[4] A. Auerbach, *Interacting Electrons and Quantum Magnetism* (1994).

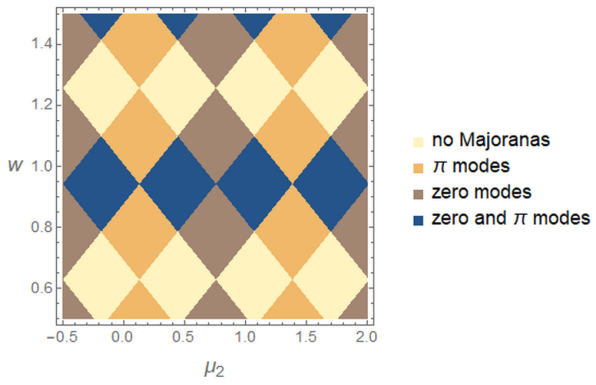

FIG. 7. The phase diagram of the stroboscopic Kitaev model when only the chemical potential μ varies between two values. Parameters, $\mu_1 = 0.5$, $T_1 = T_2 = 5$ are fixed and the phase digagram is plotted with respect to μ_2 and w. Sweet spot appear at the center of the phase diamonds similar to Fig. 1 of the main text.

[5] J. D. Sau and S. D. Sarma, Nat. Commun. **3**, 964 (2012).
[6] I. C. Fulga, A. Haim, A. R. Akhmerov, and Y. Oreg, New J. Phys. **15**, 045020 (2013).
[7] Z. Su, A. B. Tacla, M. Hocevar, D. Car, S. R. Plissard, E. P. A. M. Bakkers, A. J. Daley, D. Pekker, and S. M. Frolov, Nat. Commun. **8**, 585 (2017).
[8] L. Jiang, T. Kitagawa, J. Alicea, A. R. Akhmerov, D. Pekker, G. Refael, J. I. Cirac, E. Demler, M. D. Lukin, and P. Zoller, Phys. Rev. Lett. **106**, 220402 (2011).
[9] D. A. Abanin, W. De Roeck, and F. Huveneers, Phys. Rev. Lett. **115**, 256803 (2015), arXiv:1507.01474.
[10] M. Wimmer, ACM Transactions on Mathematical Software (TOMS) **38**, 30 (2012).
[11] S. Bravyi and D. Gosset, Commun. Math. Phys. **356**, 451 (2017), arXiv:1609.00735.
[12] B. Bauer, T. Karzig, R. V. Mishmash, A. E. Antipov, and J. Alicea, ArXiv180305451 Cond-Mat (2018), arXiv:1803.05451 [cond-mat].